Wettability versus roughness: Multi-scales approach

Vanessa Belaud, Stéphane Valette, Guy Stremsdoerfer, Maxence Bigerelle, Stéphane Benayoun

▶ **To cite this version:**

Vanessa Belaud, Stéphane Valette, Guy Stremsdoerfer, Maxence Bigerelle, Stéphane Benayoun. Wettability versus roughness: Multi-scales approach. Tribology International, 2015, 82, pp.343-349. 10.1016/j.triboint.2014.07.002 . hal-04533575

HAL Id: hal-04533575

https://uphf.hal.science/hal-04533575v1

Submitted on 5 Apr 2024

HAL is a multi-disciplinary open access archive for the deposit and dissemination of scientific research documents, whether they are published or not. The documents may come from teaching and research institutions in France or abroad, or from public or private research centers.

L'archive ouverte pluridisciplinaire **HAL**, est destinée au dépôt et à la diffusion de documents scientifiques de niveau recherche, publiés ou non, émanant des établissements d'enseignement et de recherche français ou étrangers, des laboratoires publics ou privés.

Wettability versus roughness: Multi-scales approach

V. Belaud [a,*], S. Valette [a], G. Stremsdoerfer [a], M. Bigerelle [b,c], S. Benayoun [a]

[a] Laboratoire de Tribologie et dynamique des systèmes, Ecole Centrale de Lyon, 69134 Ecully, France
[b] Laboratoire d'Automatique, de Mécanique et d'Informatique Industrielle et Humaine, LAMIH, UMR CNRS 8201, Valenciennes, France
[c] Laboratoire de Thermique, Ecoulement, Mécanique, Matériaux, Mise en Forme, Production, TEMPO, EA 4542, Valenciennes. France

ARTICLE INFO

Keywords:
Wettability
Surface texturing
Laser femtosecond
Polypropylene

ABSTRACT

These authors experimentally investigate the influence of multi-scale roughness on contact angle measurements, and they propose a model combining the Wenzel and Cassie–Baxter equations with the 3D roughness parameters defined by ISO25178. To do this, a generic methodology based on a statistical method (bootstrap and correlation coefficient) is developed and applied to a polypropylene textured femtosecond laser (55 surfaces, ablation depths = 5–45 μm and depth/diameter = 0.07–0.53). A mixed model is proposed according to the correlations obtained between the contact angle of a plane surface, θ_0, and a textured surface, θ, with the roughness parameters as the developed surface, S_{dr}, closed hills area, S_{ha} and the closed dales area, S_{da}, with regard to the models of Wenzel and Cassie–Baxter.

1. Introduction

Polymers such as polypropylene (PP) are frequently used in industrial applications, such as the automobile and cosmetics industries. However, surface treatments are necessary to improve the surface wetting and adhesion properties to permit the esthetics aspects.

Surface texturing is essential in many industrial applications, such as liquid coating, lubrification, painting, and jet-printing [1]. According to Etsion [2], laser surface texturing can produce micro-dimples on the surface and each of these can serve either as a micro-hydrodynamic bearing in cases of full or mixed lubrification or a micro-reservoir for lubricant in cases of starved lubrification conditions. We can then ask, what is the contact between the lubricant and the textured surface? Before turning to the parameters, such as the contact pressure, the wettability properties are often studied [3].

Wettability properties are usually quantified in terms of the apparent contact angle, which is the angle between the solid surface and the liquid–air interface [1].

The wettability of surfaces depends on the liquid chemical properties but can also be strongly affected by surface roughness. The first approach was made by Wenzel [4]. His theory was based on the assumption that a rough surface extends the solid–liquid interface area in comparison to a projected smooth surface. In the general case, the Wenzel theory uses the equation:

$$\cos\,\theta = r\,\cos\,\theta_0 \tag{1}$$

where θ is the apparent contact angle, and r is the ratio of the real rough surface area to the projected perfectly smooth surface. θ_0 is the contact angle corresponding to the ideal smooth surface. Another attempt to describe the surface heterogeneity was made by Cassie and Baxter [5]. The Cassie-Baxter theory proposes an equation of the apparent contact angle for the heterogeneous contact of a liquid droplet (water) on a composite surface that is composed of a solid (on an area fraction f) and air (on an area fraction $1-f$), which is

$$\cos\,\theta = f\,\cos\,\theta_0 - (1-f) \tag{2}$$

where θ_0, is the contact angle of the liquid droplet on the flat solid surface.

For real heterogeneous and complex rough surfaces, different scenarios can be obtained and described in Fig. 1. The drop can be seen on the rough surface, like in the Wenzel and Cassie–Baxter models, or as two mixed states. First, the drop follows the Wenzel model for nanometric scale roughness and the Cassie–Baxter model for micrometric scale roughness. Second, the drop follows the Wenzel and Cassie–Baxter for micrometric and nanometric scale, respectively. These scenarios can be found in the nature of super-hydrophobic surfaces, like lotus or rose leaves [6].

To describe real surfaces, different authors proposed a combination of these two theories [6,7]. The surfaces are described by 2D and 3D parameters defined by EUR15178N and ISO25178. The correlation between these parameters and the contact angle are studied [8–10]. The relevant parameters define the multi-scale surfaces; however, there is no answer to the question: "What is the pertinent scale of roughness to analyze the behavior of the interface drop-substrate?"

* Corresponding author.

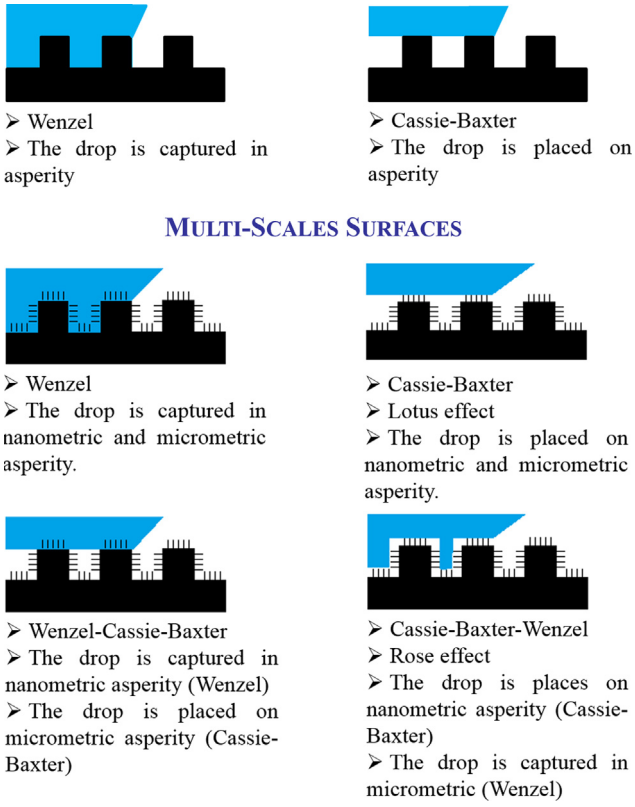

Fig. 1. Schematic of the different wetting scenarios for the roughness surface models and the multi-scales roughness surfaces, see Ref. [6].

The aim of this paper is to statistically demonstrate the relevant scale of the measurement parameters on real multi-scale surfaces created by femtosecond laser treatment in order to describe the surface wettability.

2. Experiments

2.1. Tested material

The PP used in this study was characterized by infrared spectroscopy (IRS) and differential scanning calorimetry (DSC). It is an isotactic polypropylene with a degree of crystallinity approximately 55% (measured on 10 samples). The cooling of the PP after laser treatment is considered homogenous.

2.2. Surface preparation

Tested surfaces are prepared by femtosecond laser ablation. This method presents different advantages, including a reproducible finishing process and multi-scale surface texturing [11].

The femtosecond laser source used in our experiments is a Ti laser: sapphire developed by Thales™. This laser delivers pulses with an average duration of 130 fs with a repetition rate of 5 kHz. The wavelength of the emitted light is centered around $\lambda = 800$ nm. The laser was used at normal incidence to the surface of the sample; the beam diameter is kept constant at $Ø = 60 \pm 5$ μm and is measured on a reference steel with the laser parameters, $N = 20$ and $P = 30$ mW. The beam is focused by multiple mirrors and a diaphragm, and the shape of the beam depends on the optimization of the optical path of the beam [12]. The shape of the beam obtained and used in this study is a top-hat beam with a cylindrical shape.

The different values of surface roughness were obtained by changing the lag beam, horizontal Δ_h and vertical Δ_v, (5 conditions).

($\Delta_h = 1/2\ Ø$; $\Delta_v = 1/2\ Ø$), ($\Delta_h = 1/2\ Ø$; $\Delta_v = Ø$), ($\Delta_h = 1/2\ Ø$; $\Delta_v = 2\ Ø$), ($\Delta_h = Ø$; $\Delta_v = Ø$), and ($\Delta_h = 2\ Ø$; $\Delta_v = 2\ Ø$);

the power density, P, (9 conditions).

$P = 150$ mW, $P = 200$ mW, $P = 250$ mW, $P = 300$ mW, $P = 350$ mW, $P = 400$ mW, $P = 450$ mW, $P = 500$ mW, and $P = 550$ mW;

and the number of pulses N (2 conditions).

$N = 5$ and $N = 10$.

Twelve representative surfaces are presented in Fig. 2. All specimens (55 surfaces) were prepared following the same procedure; however, due to specific laser-polypropylene interactions, the impact diameter increases with the power density [13]. The displacement of the beam, Δ_h and Δ_v, is chosen according to the impact diameter, Ø, to produce a wide range of ablation depths, $H = 5$–45 μm, and a wide range of aspect ratios, $A = 0.07$–0.53. A representation of tested surfaces is presented in Fig. 2.

The different displacements of the beam along the horizontal and vertical axis created a principal direction on 33 surfaces, called anisotropic surfaces. The other 22 surfaces are considered isotropic.

It is important to note that the product morphology can be decomposed to the form component (μm) and the roughness component (nm). The drop is posed on several grounds as representative of the surface topography. The drop and the periodic structures analyzed have the same sizes (μm). A study involving evaporation of the drop shows a strong influence on the contact drop/surface. Finally, in the study, it is considered that there is no chemical modification of the polymer after laser texturing. The treatment conditions chosen cannot distinguish the modification of the surface chemistry by IR or XPS analysis.

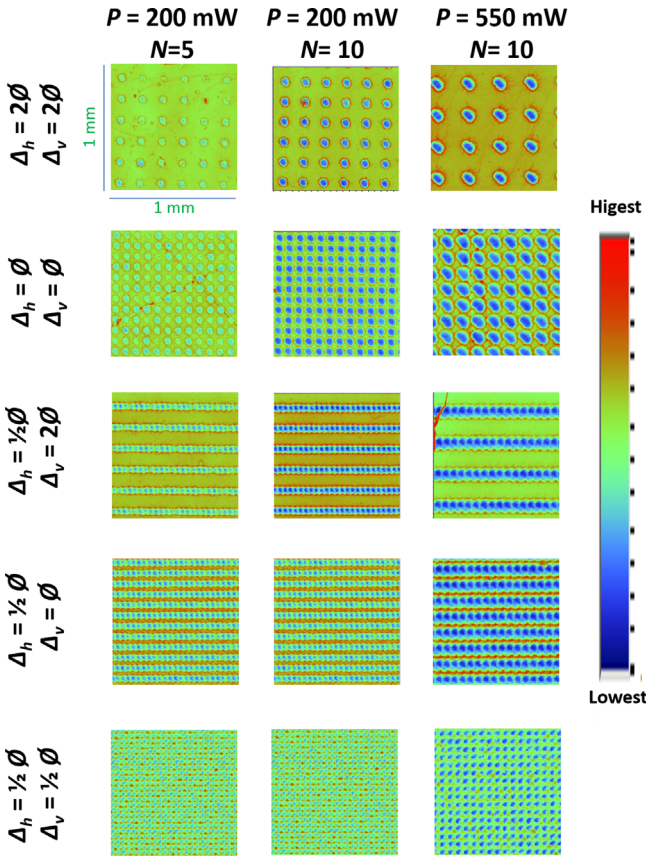

Fig. 2. Interferometric imaging of the textured surface treated by laser ablation. Each image has the same scale: 1 mm × 1 mm. The horizontal beam lag, Δ_h, the vertical beam lag, Δ_v, the power density, P, and the number of pulses are modified to obtain a range of different roughness.

2.3. Contact angle measurements

The contact angle between the water and the tested materials has been measured using the sessile drop method for both directions defined by the anisotropic samples. The principle of the measurement is presented in Fig. 3. The anisotropic properties are not the objective of this study. The contact angles are measured along the horizontal and vertical axes defined by the structuration to obtain the greater dispersion measures. The drop volume was taken within the range where the contact angle did not change with the variation of the volume (3 μL). Tests were conducted at an ambient temperature of $T \sim 22$ °C and at a relative humidity HR ~45%. The equilibrium contact angles were observed and measured rapidly ($t < 20$ s) after the drop was deposited on the polymer. During this period the evaporation of the drop water is negligible and its volume is assumed to be constant.

2.4. Surface morphology measurements

The surface roughness parameters of the treated surfaces were calculated from the topographical data measures by a 3D optical white light interferometer. The measurements were based on the non-contact vertical scanning interferometry (VSI) measurement mode with the use of an 10x objective. Six topographical measurements were performed for each analyzed surface with the following size of the measured regions (1 mm × 1 mm). These profile dimensions take into account the real surface. In fact, the surface patterns are periodic (~5 periodic patterns). Moreover, the contact area of the drop is close to 4 mm² (10–12 periodic patterns).

The topographical 3D parameters were calculated according to the following standards defined by EUR15178N and ISO25178. A total of 63 different roughness 3D parameters were calculated for all 55 tested surfaces and for 100 surfaces generated by the multi-scale decomposition for each of the 55 surfaces. This procedure generated a huge amount of data; therefore, the statistical method was used to analyze and determine the most relevant parameters that influence the contact angle measurement. The selected parameters are presented and defined in Table 1. These parameters can be associated with the Wenzel (S_{dr}) and Cassie-Baxter (S_{da}, S_{ha}) parameters r and f in the following expressions

$$r = (S_{dr} + 100)/100 \tag{3}$$

$$f = S_{ha}/(S_{ha} + S_{da}) \tag{4}$$

2.5. Multi-scales decomposition

The topography induced by the femtosecond laser is multi-scale, comprising the form and the roughness. If we set a spatial reference scale, two visions of the surface topography can be considered. The first is to quantify the form beyond this level by ignoring from the roughness measured below. The second is to analyze the roughness refraining the form. For this, a Gaussian high-pass filtering (roughness) with a cut-off, λ^H, and a Gaussian low-pass filtering (form) with a cut-off λ^L, are used. This is followed by a multi-scale decomposition. For each filter, a 50 spatial scale, λ (cut-off), is selected. Each surface gives access to 100 surfaces.

Fig. 4 shows the multi-scale decomposition for the low-pass and high-pass filters at different scales (λ_i=220 and λ_i=40 μm) and one type of surface that is fairly representative of the extent of the surfaces studied. Fig. 4 shows the 2D profiles corresponding to the surface Δ_h=1/2 Ø, Δ_v=2Ø. The first profile (λ^L=220 μm) presents a sinusoidal profile. When the cut-off is λ^L=40 μm, the profile contains more details. On this profile, the edges of impact are present. The profile obtained with $\lambda^L < 40$ μm has a roughness added to the form. These different stages are found for other surfaces. The first filter (high λ^L) introduces the form component of the profile, whereas filters at smaller scales introduce the roughness added to the form (Fig. 4(a)). With low-pass filtering, the smallest scale gives access to the integral profile.

Unlike with high-pass filtering, the highest scale gives access to the integral profile, as seen in Fig. 4(b). This figure shows the 2D profiles corresponding to the surface Δ_h=1/2 Ø, Δ_v=2Ø with a high-pass filter. The first profile (λ^H=220 μm) presents a profile compound of the shape and the roughness. When we decrease the cut-off (λ^H=40 μm), the form disappears in favor of the roughness. We can see that the roughness is higher in the laser-modified are.

After this decomposition, each surface corresponds to 100 different surfaces, for which the 3D roughness parameters can be calculated. Fig. 5 shows the evolution of the S_{dr} parameters according to the scale decomposition (λ^L and λ^H). We see two regimes with a transition λ_i ~45 μm corresponding to half the impact diameter, Ø. For the high-pass filter, the filters less than $\lambda^H < 50$ μm characterize the roughness with a fractal structure type [14]. For $\lambda^H > 50$ μm, the structures are of the Euclidian type, and S_{dr} characterizes the macroscopic morphology that seems does not depend on the shape. The evolution of S_{dr} is then constant.

2.6. Statistical analysis (bootstrap and standard deviation)

In this section, we present an original methodology developed to investigate the nature of the relationship between a roughness parameter taken at a given spatial scale using a standard filter set (high-pass or low-pass) and the wettability properties. The objective is to determine the most relevant roughness parameters (63 3D parameters), filtered to an optimal scale (50 cut-off, (λ_i, for each filter)) using the best filter (high-pass or low-pass).

Table 1
Syntheses of the most relevant morphological parameters that influence the wetting phenomenon, selected by statistical analysis.

3D parameters (EUR 15178N; ISO25178)		Correlation coefficient
S_{ha}	Closed hills area	0.85
S_{da}	Closed dales area	0.85
S_{dr}	Developed area ratio	0.84
S_{sk}	Skewness of height distribution	0.83

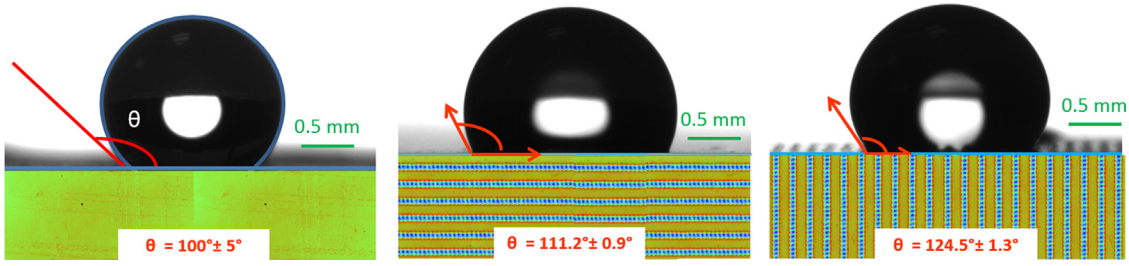

Fig. 3. Representation of the experimental measurements of the contact angle on a smooth surface and a textured surface in both directions of the surface texture.

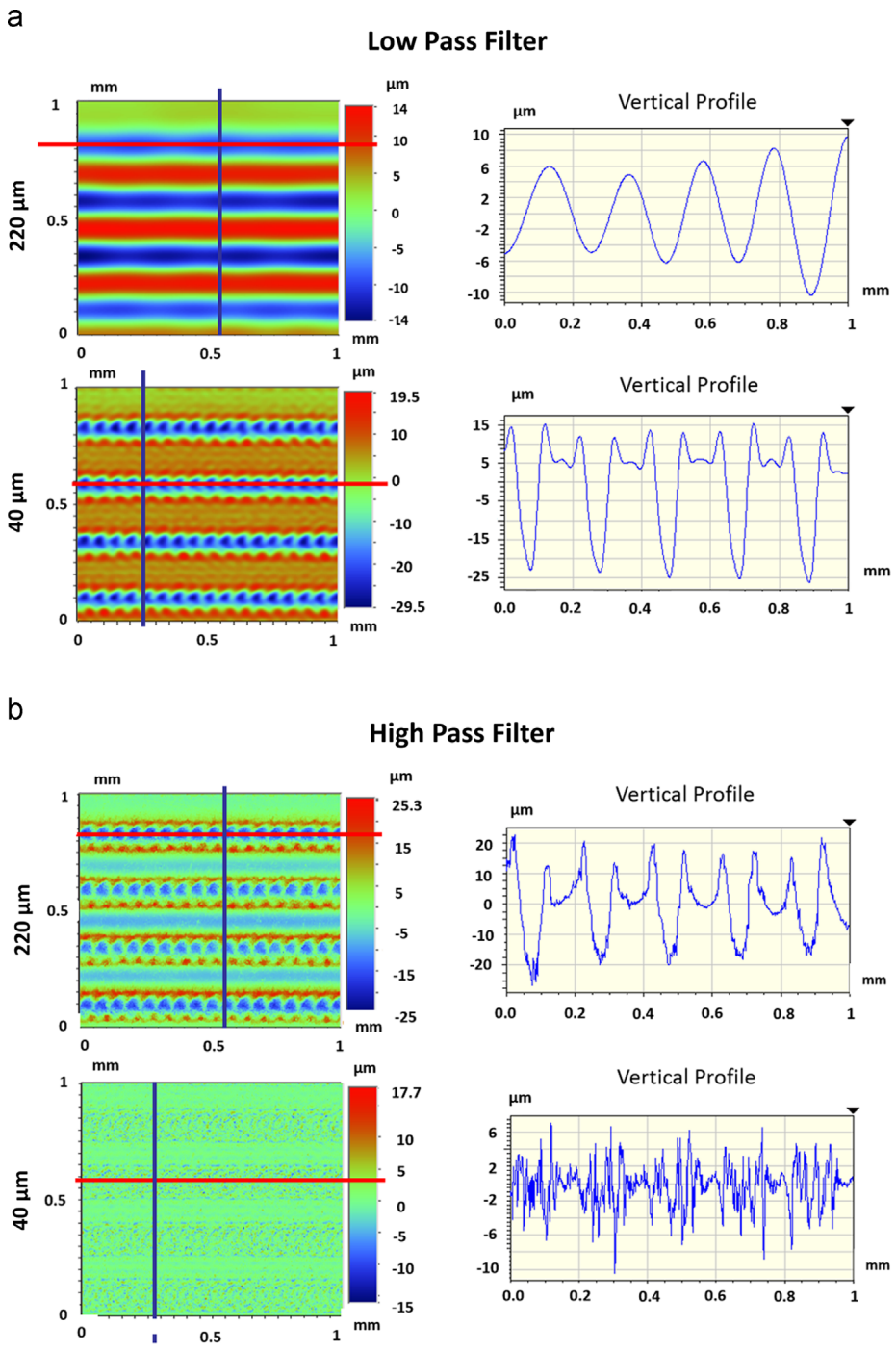

Fig. 4. Examples of multi-scales decomposition by a low pass filter (a) and a high pass filter (b) for two surface morphologies representative of all the surfaces. The blue line indicates the vertical direction, and the red line indicates the horizontal direction. The map and the profile are calculated for two values of cut-off, λ_i=220 µm and λ_i=40 µm, and two filters. (For interpretation of the references to color in this figure legend, the reader is referred to the web version of this article.)

We propose to illustrate this sequential method using roughness parameters, $S_{dr,}$ calculated at the whole scale, and the contact angle, θ, for 5 textured surfaces ((Δ_h=1/2 Ø; Δ_v=1/2 Ø), (Δ_h=1/2 Ø; Δ_v=Ø), (Δ_h=1/2 Ø; Δ_v=2 Ø), (Δ_h=Ø; Δ_v=Ø), and (Δ_h=2 Ø; Δ_v=2 Ø)) with laser parameters, P=300 mW and N=10.

The search for a phenomenological model involves several steps:

(1) To determine the estimated uncertainties of the experimental values.
(2) To search for the scale relevant for each 3D parameter.
(3) To search for a relationship between the roughness parameters and the contact angle.

The measured data (contact angle and roughness parameters) are independent. To write a relationship between these quantities, it is necessary to reduce the data of each quantity, usually to their average. In this case, the value corresponds to the variability of the experimental values estimated by the bootstrap analysis [15,16]. The bootstrap analysis allows for estimation of the sampling

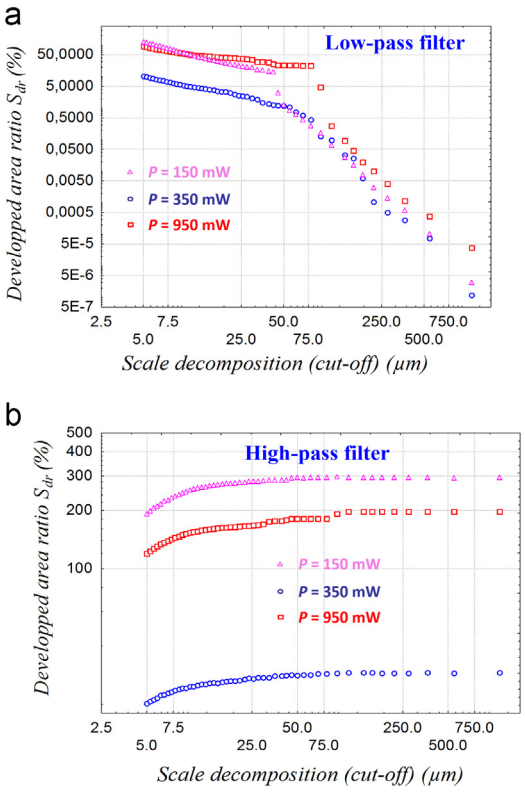

Fig. 5. Evolution of the 3D parameter S_{dr} according to the scale decomposition (cut-off) with (a) low-pass and (b) high-pass Gaussian filters for representative surfaces.

distribution by resampling methods. One standard choice for an approximating distribution is the average of the measurements. Each average is obtained by random sampling in the original data. A total of 100 000 drawings are made from the surface.

Fig. 6(a) shows the variability of the roughness parameters, S_{dr}. The averages are strictly different. However, in Fig. 6(b), the variability of the contact angle, θ, is not statistically distinguishable, except for the surface with $\Delta_h = \Delta_v = 2\emptyset_i$. This result causes a strong dispersion in the analysis of the results presented in Fig. 10.

Fig. 7 presents the classification of all the roughness parameters, at all scales, versus the correlation coefficient [17] between the roughness parameters and the contact angle. The roughness parameters, S_{ha} and S_{da}, are relevant ($R^2 = 0.85$) for a low-pass filter with $\lambda^L = 40$ μm, and S_{dr} is relevant ($R^2 = 0.84$) for a high-pass filter with $\lambda^H = 220$ μm.

3. Results and discussion

Different approaches are possible to determine the relationship between the roughness parameters and the contact angle. The first consists of using the classical model with the roughness parameters, like the $r = f(S_{dr})$ of (Wenzel) and the $f = f(S_{ha})$ of Cassie–Baxter. We can see in Fig. 8 that these models do not correspond to the experimental results. The scatter of the experimental data suggests, in Fig. 8 and the following Figs. 9.and 10, poor precision of the collected data. This dispersion is explained by Fig. 6. We can see that despite the differentiation of the surfaces by the roughness parameter S_{dr}, which is very sensitive to micro-cavities, the contact angle does not allow differentiation of the resulting contact angles for different S_{dr}.

In the previous section, we have shown in Fig. 7 that the S_{dr} is relevant for a scale of $\lambda^H = 220$ μm with a high-pass filter, and S_{ha}

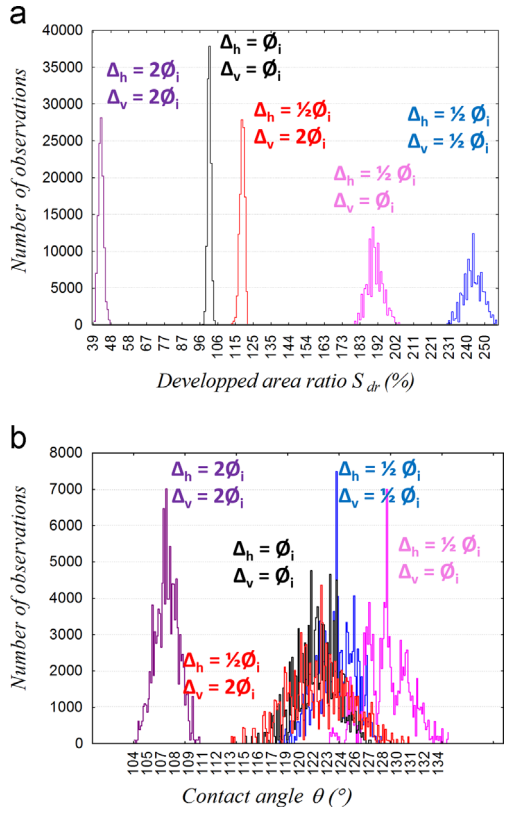

Fig. 6. Distributions of the experimental values for (a) the developed area ratio, S_{dr}, and (b) the contact angle, θ. These data are obtained on different surface textures with $P=300$ mW and $N=10$ with different beam lags Δ_h, and Δ_v.

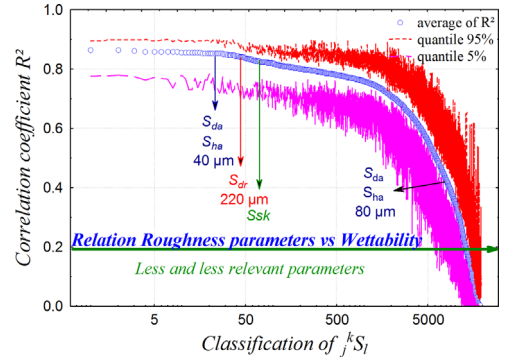

Fig. 7. Classification of the correlation coefficient between the contact angle θ and the roughness parameters, $^{k}_{j}S_{l}$, where j indicates the cut-off, k indicates the type of Gaussian filter, and l indicates the type of roughness parameters.

and S_{da} are relevant for a scale of $\lambda^L=40$ µm with a low-pass filter. Fig. 9 shows the Wenzel and Cassie–Baxter models with the roughness parameters calculated at relevant scales. The Wenzel model is not always appropriate, but the Cassie–Baxter model shows a better correlation.

A mixed model based on the Cassie–Baxter and Wenzel theories is proposed. Fig. 7 shows a high correlation coefficient between S_{dr} and θ when $\lambda^H<50$ µm, and only the roughness component, as seen in Fig. 4. This leads us to say that the roughness is important only on the bottom of the hills. The developed area ratio at this scale is $r^H=(S_{dr}+100)/100$.

Moreover, S_{ha}, which characterizes the Cassie–Baxter model, is relevant for $\lambda^L>40$ µm with a low-pass filter, a scale that takes into account the component form, as seen in Fig. 4. In this way, it is possible to determine a fraction of the "microscopic" area on which the drop is in contact with the polymer, $f^L=S_{ha}/(S_{ha}+S_{da})$.

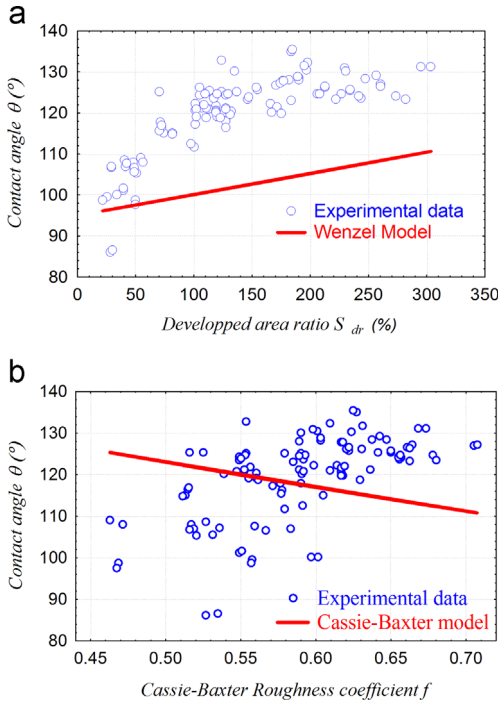

Fig. 8. Contact angle versus roughness parameters calculated at the whole scale (a) Comparison of the Wenzel model, $\cos\theta=r\ ^*\cos(\theta_0)$, and experimental data. (b) Comparison of the Cassie–Baxter model, $\cos\theta=f\cos(\theta_0)-(1-f)$, and experimental data, where $f=S_{ha}/(S_{ha}+S_{da})$, $r^H=(S_{dr}+100)/100)$, and θ_0 is the contact angle on a flat surface of the polymer.

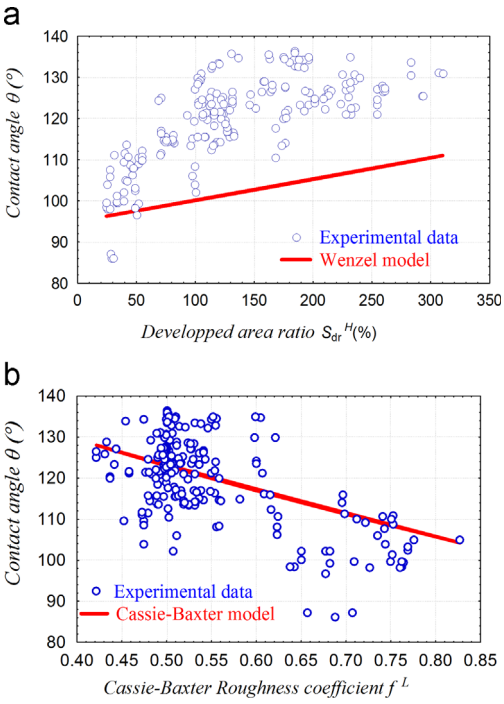

Fig. 9. Contact angle versus roughness parameters calculated at their relevant scale (a) Comparison of the Wenzel model, $\cos\theta=r^H\ ^*\cos(\theta_0)$, and the experimental data. (b) Comparison of the Cassie–Baxter model, $\cos\theta=f^L\cos(\theta_0)-(1-f^L)$, and experimental data, where $f^L=S_{ha}/(S_{ha}+S_{da})$, $r^H=(S_{dr}+100)/100)$, and θ_0 is the contact angle on a flat surface of the polymer.

From Eq. (2), the relation of the apparent contact angle versus the topographic parameters that we proposed is

$$\cos\theta=f^L(r^H\cos\theta_0)-(1-f^L) \tag{5}$$

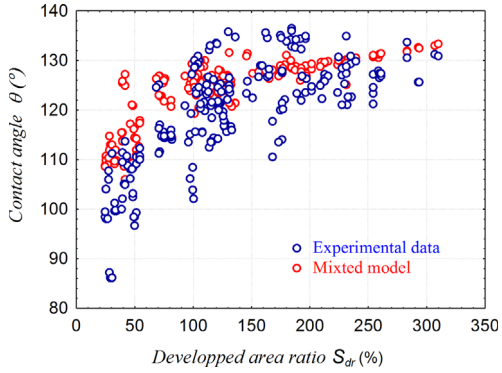

Fig. 10. Contact angle versus roughness parameters calculated at their relevant scale. Comparison between the experimental data and the developed mixed model according to the equation $\cos\theta = \cos\theta = f^L\ (r^H\ \cos\ \theta_0) - (1 - f^L)$,where $f^L = S_{ha}/(S_{ha}+S_{da})$, $r^H = (S_{dr}+100)/100$, and θ_0 is the contact angle on a flat surface of the polymer.

where θ_0 is the contact angle on the smooth surface of polypropylene (95°).

Fig. 10 shows the comparison between the experimental data and this mixed model. This model describes the Wenzel–Cassie–Baxter Model presented in Fig. 1.

We also mentioned that several surfaces are anisotropic; they present a main direction. Note that the contact angles obtained in the main direction of texturing are greater than the theoretical values. The model predicts the average value obtained by both directions.

4. Conclusion

An experimental investigation of the static contact angle measured on polypropylene textured surfaces by a femtosecond laser with multi-scales roughness shows the dependence of the 3D roughness parameters S_{dr}, S_{ha} and S_{da}.

The 3D profile of the multi-scales textured surfaces are decomposed by a Gaussian high-pass and low-pass filter for 50 different cut-offs, λ_i. The statistical analysis showed that S_{dr} is relevant for a scale of $\lambda^H < 220\ \mu m$ for a high-pass filter, and S_{ha} and S_{da} are relevant for a cut-off $\lambda^L > 40\ \mu m$ with a low-pass-filter. The roughness parameter S_{dr} is relevant to describe the roughness of the textured surface, and the parameters, S_{ha} and S_{da} are relevant for the form component description of the profile.

The proposed physical approach shows that the drop is not in the state described by Wenzel or Cassie–Baxter, even with the roughness parameters calculated at the relevant scales. Finally, the authors proposed a model using both approaches.

The proposed model depends on the roughness parameters S_{dr}, S_{ha} and S_{da} for the relevant scales. Several conditions are required: the polymer surface is chemically homogenous, the parameter calculation is performed on a similar surface to the contact surface of the drop and the cut-off of the filters associated with the roughness parameters are small compared to the drop diameter.

The proposed mixed model expression is

$$\cos\ \theta = f^L(r^H\ \cos\ \theta_0) - (1 - f^L)$$

where $f^L = S_{ha}/(S_{ha}+S_{da})$, $r^H = (S_{dr}+100)/100$, and θ_0 is the contact angle on a flat surface of the polymer.

Further investigations are needed to validate this approach for different materials and textures.

References

[1] De Gennes PG. Wetting: statics and dynamics. Rev Mod Phys 1985;57(3):827.
[2] Etsion I. State of the art in laser surface texturing. J Tribol 2005;248:127.
[3] Pawlak Z, Urbaniak W, Oloyede A. The relationship between friction and wettability in aqueous environment. Wear 2011;271:1745.
[4] Wenzel RN. Resistance of solid surfaces to wetting by water. Ind Eng Chem 1936;28:988.
[5] Cassie ABD, Baxter S. Wettability of porous surfaces. Trans Faraday Soc 1944;40:546.
[6] Nosonovsky M, Bhushan B., Lotus versus rose: biomimetic surface effects, chapter 2, green tribology (2012).
[7] Kubiak KJ, Wilson MCT, Mathia TG, P.h. Carval. Wettability versus roughness of engineering surfaces. Wear 2011;271:523.
[8] Kubiak KJ, Mathia TG, Wilson MCT. Methodology for metrology of wettability versus roughness of engineering surfaces. In: Proceedings of 14th Congrès International De Métrologie. Paris; 22nd–25th June 2009.
[9] Kubiak KJ, Wilson MCT, Mathia TG, Carras S. Dynamics of contact line motion during the wetting of rough surfaces and correlation with topographical surface parameters. Scanning 2011;33:370.
[10] Ourahmoune R, Salvia M, Mathia TG, Mesrati N. Surface morphology and wettability of sandblasted PEEK and its composites. Scanning 2013 (Online).
[11] Bizi-Bandoki P, Benayoun S, Valette S, Beaugiraud B, Audouard E., Modifications of roughness and wettability properties of metal induced by femtosecond laser treatment, Appl Surf Sci, 257: 5213.
[12] Rosenfeld A, Lorenz M, Stoain R, Ashkenasi D. Ultrashort-laser-pulse damage threshold of transparent materials and the role of incubation. Appl Phys A 1999;69:S373–6.
[13] Belaud V, Valette S, Stremsdoerfer G, Beaugiraud B, Audouard E, Benayoun S. Femtosecond laser ablation of polypropylene: a statistical approach of morpholnical Data. Scanning 2013 (Online).
[14] Lewis F. Richardson. The problem of contiguity: an appendix to statistic of deadly quarrels. General systems: yearbook of the society for the advancement of general systems theory. (Ann Arbor, Mich.: The Society, [1956-: Society for General Systems Research) 6 (139);1961. p. 139–187.
[15] Efron B, Tibshirani RJ. An introduction to the Bootstrap. Chapman & Hall; 1994.
[16] Peter Hall. The bootstrap and Edgeworth Expansion, Springer series in Statistics.
[17] Tufféry S., Data mining et statistique décisionnelle: l'intelligence des données (2010) Editions Technip.